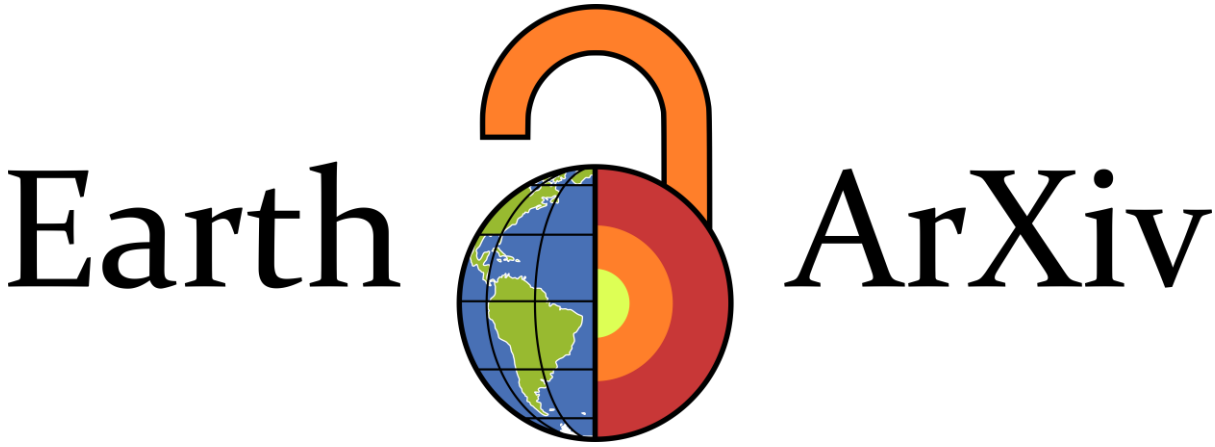

National scale sub-meter time series mangrove mapping using Landsat imagery and deep transfer learning

Junkai Ma[1,※], Chunyuan Diao[4,※], Jinyan Tian[1,2,3,*], Meng Xu[1], Mingming Jia[5], Chen Shi[1], Jie Song[1], Zhaorong Liu[1], Jiahuan Liu[1], Wei Chen[1], Songzhao Mei[1], Xiumin Zhu[1], Niu Luo[1], Lin Zhu[2,3]

[1]Key Laboratory of 3D Information Acquisition and Application, Ministry of Education, Capital Normal University, Beijing, 100048, China

[2]Beijing Laboratory of Water Resources Security, Capital Normal University, Beijing, 100048, China

[3]Jing-Jin-Ji Geospatial Data Center, Capital Normal University, Beijing, 100048, China

[4]Department of Geography and Geographic Information Science, University of Illinois at Urbana-Champaign, Urbana, IL 61801, USA

[5]Key Laboratory of Wetland Ecology and Environment, Northeast Institute of Geography and Agroecology, Chinese Academy of Sciences, Changchun, 130102, China

※These authors contributed equally to this work.

*Correspondence to: Jinyan Tian (tjyremote@126.com)

Abstract

Current mangrove time-series products are constrained to 25 m resolution, hindering precise delineation of boundaries, small patches, and internal structures, thus compromising area estimates and ecological assessments. Key barriers are the paucity of historical high-resolution imagery and high-quality labeled samples. To this end, we developed the Sub-meter Mangrove Transfer Learning Mapping (SMTLM) framework, combining a pre-trained model from 2020 existing sub-meter products with transfer

fine-tuning using few-shot samples from target historical years. We resampled time-series Landsat imagery to sub-meter resolution and selected proven spectral bands and vegetation indices. To improve temporal transferability, we designed and evaluated three strategies: direct transfer learning (DTL), partial fine-tuning (PFT), and layer-wise fine-tuning (LFT). SMTLM generated China's first national Sub-meter Time-series Mangrove Map (STMM) for 1990-2020, achieving overall accuracy of 93.4%-97.2% and F1-scores of 0.93-0.97. STMM indicates a 105% mangrove area increase from 2000 (14,316 ha) to 2020 (29,413 ha), nearly five times the 23.3% from existing product. When benchmarked against STMM, existing product exhibit commission and omission errors totaling 9,496–19,089 ha, and STMM detecting 2-4 times more mangrove patches. SMTLM provides a scalable solution for sub-meter mapping under sample-limited conditions, enhancing temporal transferability of high-resolution methods. STMM offers a long-term, high-resolution dataset for precise mangrove dynamics assessment, revealing far greater 21st-century recovery in China than previously recognized. Optimized 30 m Landsat imagery via SMTLM retrieves fine spatial details comparable to sub-meter results, highlighting sub-meter mapping's improvement over existing coarse-resolution products for reliable monitoring.

1. Introduction

Mangroves are among the most carbon-rich forest ecosystems globally (Wang et al., 2019), providing critical coastal protection, biodiversity habitat, and carbon sequestration (Giri et al., 2015; Xu et al., 2024). However, they face accelerating degraded from anthropogenic activities and climate change (Chen et al., 2017; Hu et al., 2018), with a global decline of 524,500 ha from 1996 to 2020 (Bunting et al., 2022). Given their ecological significance and conservation urgency, accurate and long-term monitoring of mangroves is urgently needed. Compared with traditional field surveys, remote sensing enables cost-effective, large-scale, and long-term monitoring of mangrove distribution (Tian et al., 2017; Zhao and Qin, 2020).

Large-scale mangrove mapping studies are categorized by spatial resolution into

high-resolution (HR, 10-30 m) and very high-resolution (VHR, <10 m). HR imagery (e.g., Landsat and Sentinel-2) benefits from open access and extensive temporal coverage, making it widely used for long-term, large-scale monitoring (Hamilton and Casey, 2016; Zhao and Qin, 2020). The Global Mangrove Watch (GMW) dataset has become a widely adopted global baseline for mangrove mapping. It provides 30-m resolution maps from 1996 to 2020, enabling consistent long-term monitoring (Bunting et al., 2018), but its coarse resolution cannot capture fine-scale spatial details. The recently released 10-m High-resolution Global Mangrove Forests (HGMF) product for 2020 markedly improves spatial detail (Jia et al., 2023). However, 10-m products face three challenges. First, precise delineation of mangrove boundaries is hindered by mixed pixels (Yang et al., 2022). Second, omission of internal structures (e.g., creeks and open spaces) critical for hydrological and ecological assessment (Matos et al., 2020). Third, small mangrove patches are often below the pixel scale and thus easily misclassified as co-existent species. These limitations result in biased estimates of area and spatial distribution, highlighting the urgent need to develop higher-resolution products (Tian et al., 2025).

VHR mangrove mapping has garnered increasing attention for its superior spatial detail and classification accuracy. For example, Zhang et al. (2021) created a 2-m resolution Mangrove Map of China 2018 using Gaofen-1 and Ziyuan-3 imagery with object-based analysis and manual editing. However, the high cost and restricted availability of these data constrain broader adoption. Another notable VHR product is the Large-scale Sub-meter Mangrove Map (LSMM) by Tian et al. (2025), the first sub-meter resolution dataset for China in 2020, generated from publicly available Google Earth and Sentinel-2 imagery. Compared to 10-m products, LSMM enhances spatial accuracy and area estimation. Nevertheless, it relies on RGB features from historical sub-meter imagery and on same-year 10-m mangrove products to derive training samples, which are not always available across time and space, thereby limiting its long-term applicability.

VHR long-term mangrove mapping encounters two primary challenges: mixed pixels in historical imagery and scarcity of high-quality historical samples. To mitigate

the first, resampling and interpolation can diminish mixed-pixel impacts on spatial boundaries, enhancing visual continuity and alignment with actual distributions (Li et al., 2022a, Chen et al., 2024). To mitigate sample scarcity, deep transfer learning provides a effective approach by integrating cross-year knowledge (Zhuang et al., 2020). The general strategy involves training a generalized model on ample samples from a specific year and transferring it to sample-scarce target years for mapping (Zhang et al., 2021). Transfer learning commonly employs three typical strategies in remote sensing: direct transfer learning (DTL), partial fine-tuning (PFT), and layer-wise fine-tuning (LFT). DTL directly applies a pre-trained model to target data without additional training, yielding low computational cost and acceptable accuracy when target samples are absent, particularly in cross-year or cross-region crop classification (Lei et al., 2024). PFT freezes shallow layers to preserve general features while updating deeper layers with limited target-year samples for domain adaptation, achieving success in land cover classification (Naushad et al., 2021). LFT progressively unfreezes layers from deep to shallow during training, enabling full parameter adaptation and demonstrating strong performance in forest species classification (Tan et al., 2025). However, mangrove mapping poses unique challenges. Spectral and spatial heterogeneity is particularly pronounced: mangroves exhibit substantial variation in species composition and age structure, and their external boundaries are often irregular due to tidal inundation (Ye and Weng, 2025). Mangrove areas also frequently overlap with unvegetated surfaces (e.g., mudflats and open water) (Tran et al., 2022) and with other vegetation types such as reeds, *Spartina alterniflora*, and Suaeda salsa (Chen and Shi, 2023; Zhou et al., 2024). To our knowledge, this issue has not yet been explicitly addressed. Therefore, applying transfer learning to achieve long-term, high-precision mangrove mapping remains a challenging yet promising research direction.

This study presents the Sub-meter Mangrove Transfer Learning Mapping (SMTLM) framework to determine the optimal transfer learning strategy for very-high-resolution (VHR) mangrove mapping. Applying SMTLM, we produced annual sub-meter mangrove maps for China from 1990 to 2020. The objectives were to: (1) assess transfer learning strategies for multi-decadal mapping and identify the best-performing

approach; (2) generate China's first Sub-meter Time-series Mangrove Map (STMM) using the superior model; and (3) benchmark STMM with existing datasets and investigate mangrove spatio-temporal dynamics over three decades. SMTLM mitigates historical samples scarcity, enabling robust VHR mangrove monitoring across decades. The resulting STMM fills a major gap in long-term sub-meter records for China, providing critical data for spatio-temporal analysis and ecological health assessment.

2. Materials and methods

2.1 Study area

Mangrove forests in China are distributed along the southern and southeastern coasts, including Hong Kong, Macao, Taiwan, Guangxi, Hainan, Guangdong, Fujian, and Zhejiang. As shown in Fig. 1, a 10-km coastal buffer zone was generated from shoreline data. The red area indicates the potential mangrove distribution zone, delineated by integrating publicly available datasets (Section 2.2.2) and augmented through visual interpretation of high-resolution and historical Google Earth imagery to include omissions. These distribution patches were consistently applied across all study years, with analyses confined to this region.

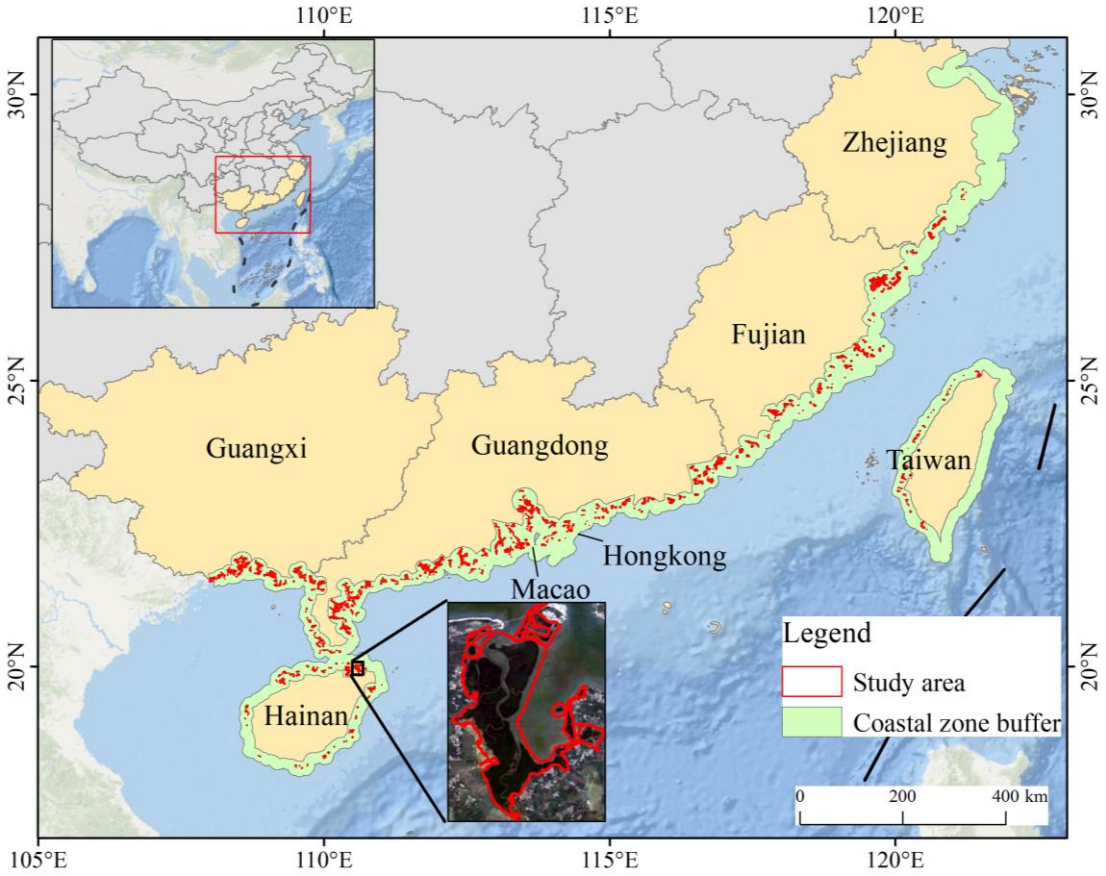

Fig. 1. Spatial extent of the mangrove study region along China's coast.

2.2 Datasets

2.2.1 Landsat imagery

This study employed Landsat 5 TM and Landsat 8 OLI surface reflectance data from Google Earth Engine (GEE). Cloud and shadow interference was mitigated using scene-based and pixel-based masking (Tian et al., 2020). Scene-based masking excluded images containing more than 70% cloud cover. Pixel-based masking applied bitwise operations to the QA_PIXEL band, targeting cloud (bit 3) and shadow (bit 4) pixels. For target-year data gaps due to persistent clouds, composites integrated cloud-free pixels from adjacent years. For example, 2020 composites used valid Landsat 8 imagery from 2019-2021, assuming negligible mangrove change during this period.

2.2.2 Available mangrove datasets

The Large-scale Sub-meter Mangrove Map (LSMM) by Tian et al. (2025) served as the reference dataset for 2020 model pre-training and accuracy assessment. Derived from Sentinel-2 and sub-meter Google Earth imagery using random forest classification and object-based segmentation, LSMM provides 0.9 m spatial resolution, 97.56% overall accuracy, and an F1-score of 0.98, and constitutes the earliest national-scale mangrove map at sub-meter resolution in China. It is publicly available at https://doi.org/10.57760/sciencedb.18643. Other historical mangrove products were collected to define the study area and enable comparative analysis (Table 1).

Table 1

Overview of the reference datasets used.

Reference	Product	Resolution	Extent	Period
Bunting et al. (2022)	Global Mangrove Watch (GMW)	30-m	Global	1996-2020
Jia et al. (2018)	Chinese Academy of Sciences Mangroves (CAS)	30-m	China	1990-2020
Zhang et al. (2021)	Mangrove China (MC)	2-m	China	1990-2018
Jia et al. (2023)	High-resolution Global Mangrove Forests (HGMF)	10-m	Global	2020
Tian et al. (2025)	Large-Scale Sub-meter Mangrove Map (LSMM)	0.9-m	China	2020

2.2.3 Reference data

To ensure robust model training and reliable evaluation, three complementary datasets were constructed: pre-training, fine-tuning, and testing. The pre-training dataset establishes a broad feature foundation using large-scale samples; the fine-tuning dataset employs limited historical sub-meter imagery for cross-year adaptation; the

testing dataset provides independent validation points for accuracy assessment. Details of their construction follow.

The pre-training dataset was derived from LSMM, converted to raster labels (mangrove = 1, background = 0). Labels and corresponding 2020 Landsat composites were divided into 512 × 512 samples, yielding 18,034 total (9,186 Guangdong, 4,665 Guangxi, 2,154 Hainan, 1,108 Fujian, 850 Taiwan, 71 Zhejiang), split 8:2 for training and validation.

The fine-tuning dataset used limited historical sub-meter imagery, segmented via multi-scale methods and visually interpreted with contemporaneous high-resolution products to generate high-quality labels. These and annual Landsat composites were partitioned into 512 × 512 samples, split 8:2; sample counts per year are detailed in Table 2.

The testing dataset comprised 10,000 validation points per year, evenly distributed across the study area with 1:1 mangrove to non-mangrove ratio. Non-mangrove samples were subdivided into mudflats, water bodies, and other vegetation types, generated using existing products and Landsat imagery.

Table 2

Sample counts for the pre-training dataset (2020) and fine-tuning dataset (other years).

Year	Sample	Train	Validation
2020	18034	14428	3606
2016	4644	3715	929
2012	5957	4765	1192
2008	7813	6250	1563
2004	4133	3307	826
2000	4924	3939	985
1990	3356	2686	670

2.3 Transfer learning framework for sub-meter mangrove mapping

To address the scarcity of high-quality historical samples in long-term mangrove mapping, we propose the Sub-meter Mangrove Transfer Learning Mapping (SMTLM) framework. As shown in Fig. 2. It comprises three components: (1) generating composite imagery by integrating Landsat data with vegetation indices and resampling; (2) pre-training a SegFormer model on 2020 samples; (3) fine-tuning with limited target-year samples. This yields a consistent time series of sub-meter mangrove maps.

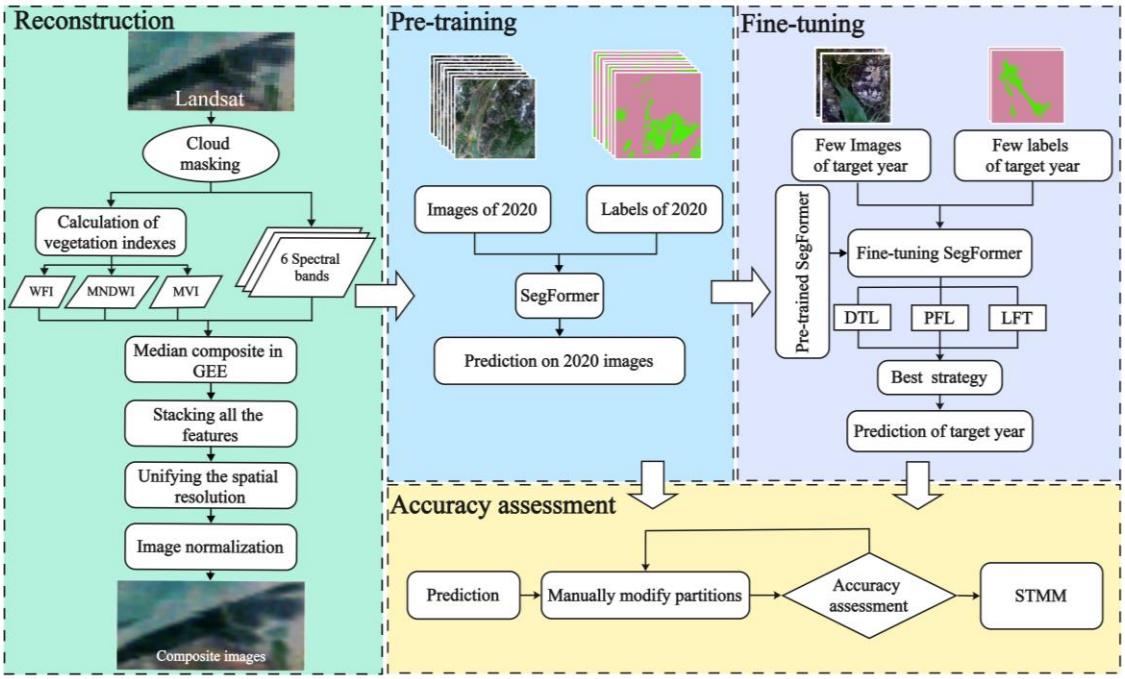

Fig. 2. Framework of Sub-meter Mangrove Transfer Learning Mapping.

2.3.1 Image reconstruction

Each Landsat image includes six spectral bands: blue, green, red, near-infrared (NIR), shortwave infrared 1 (SWIR 1), and shortwave infrared 2 (SWIR 2). From these, three vegetation indices were derived: Wetland Forest Index (WFI), Modified Normalized Difference Water Index (MNDWI), and Mangrove Vegetation Index (MVI), to enhance discrimination of mangroves from other wetlands, water bodies, and vegetation. All bands and indices were combined using median compositing in GEE, resampled to 0.9 m with cubic convolution to match the sample resolution, and scaled with min–max normalization, yielding composites with improved spectral detail and

spatial consistency with the sub-meter samples.

2.3.2 Pre-training for VHR feature learning

This study employed SegFormer, pre-trained on a large-scale dataset broadly covering the study region (Section 2.2.3). This pre-training stage enables the network to learn stable relationships between diverse image patterns and mangrove occurrence, capturing generalized spectral, spatial, and textural representations that enhance model generalization and provide a strong basis for subsequent fine-tuning.

SegFormer is a semantic segmentation network that combines the strengths of Vision Transformers (ViT) and Convolutional Neural Networks (CNN) (Fig. 3). It excels in feature extraction and spatial structure modeling (Xie et al., 2021), addressing mangrove remote sensing challenges like complex boundaries, fragmented small patches, heterogeneous internal structures, and temporal variability. SegFormer departs from standard ViT architectures by discarding positional encoding, thereby reducing the amplification of minor spatial misalignments in multi-temporal imagery. Its hierarchical Transformer uses convolutional embeddings to capture spatial relationships without fixed indices, enhancing robustness and adaptability. The lightweight MLP decoder improves inference efficiency and boundary precision while preserving fine VHR details. A hybrid attention mechanism fuses local cues for accurate edge extraction with global context for better mangrove-environment relationships, thereby improving class separability and suitability for intertidal mangrove mapping.

As shown in Fig. 3, the input image is represented as (H × W × C), where H and W are spatial dimensions and C denotes multispectral bands; initial size is 512 × 512 × 9. The encoder progressively reduces spatial resolution while increasing channel depth, and the decoder fuses and upsamples multi-scale features to restore resolution and yield pixel-level predictions. The output is 512 × 512 × 2, corresponding to mangrove and non-mangrove classes.

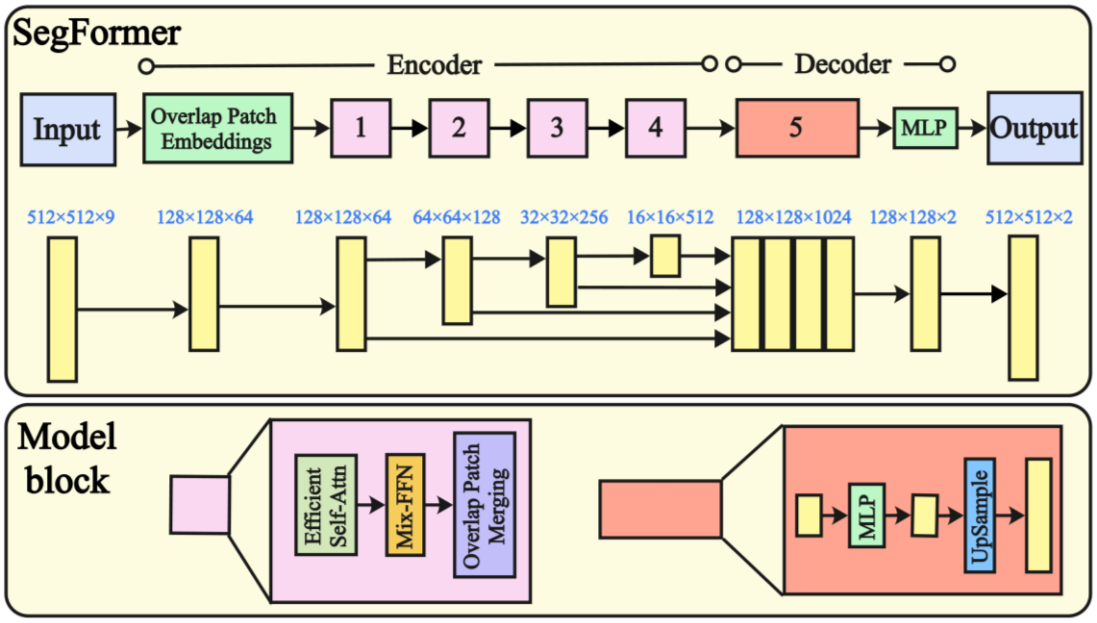

Fig. 3. SegFormer architecture and block structure.

2.3.3 Transfer learning strategy for cross-year mapping

Long-term mangrove mapping is challenged by the scarcity of high-quality historical samples. Transfer learning transfers knowledge from pre-trained models to target years under limited sample conditions, substantially reducing dependence on extensive historical training data. Existing transfer learning strategies primarily include direct transfer learning (DTL), partial fine-tuning (PFT), and layer-wise fine-tuning (LFT).

As shown in Fig. 4, DTL is applied without additional training. PFT freezes most model parameters and updates only deeper layers, preserving pre-trained low-level feature extraction while adapting to task-specific traits. In the SegFormer architecture, encoder Blocks 1-3 remain frozen as general-purpose extractors, while Block 4 and the decoder (Block 5) are fine-tuned using target-year samples at a fixed learning rate of 1e-4. This moderate rate enables efficient feature learning while mitigating overfitting risks under limited samples. Experiments employed 300 epochs for PFT, sufficient for convergence. LFT progressively unfreezes layers from deeper to shallower, offering refinement between partial and full fine-tuning. Specifically, only the decoder is trained in epochs 1-100 at 1e-4, with the encoder frozen; Blocks 3 and 4 are unfrozen in epochs

101-200 at the same rate; and all encoder blocks are unfrozen in epochs 201-300, with the rate decaying to 3e-5. This staged approach ensures stable knowledge transfer, gradual adaptation to temporal heterogeneity in remote sensing imagery, and convergence without oscillation.

Fine-tuning was performed separately for each year, and the optimal strategy was selected based on validation accuracy to generate the corresponding mangrove maps.

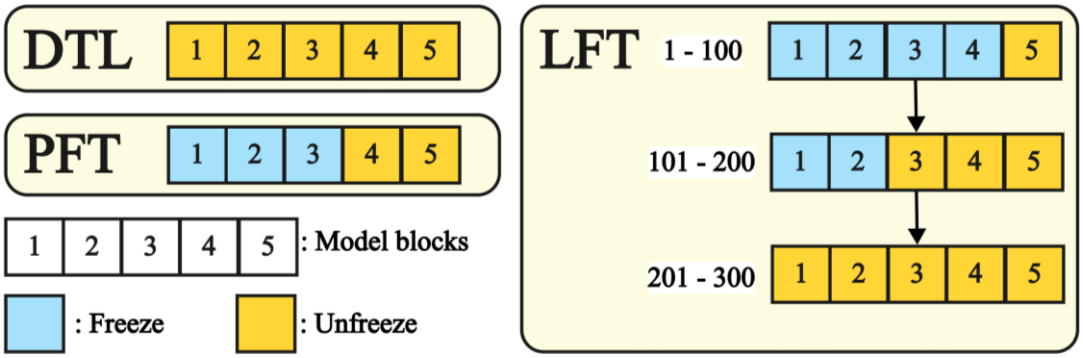

Fig. 4. Schematic diagram of freezing with different transfer learning strategies, including DTL, PFT, and LFT.

2.3.4 Sub-meter time-series mangrove map

After pre-training and fine-tuning, an annual optimal model was used to generate STMM. During inference, a sliding window partitioned each composite into 512×512 pixel tiles, which were passed through the encoder–decoder network to produce pixel-wise probability maps; pixels were assigned to the class (mangrove or non-mangrove) with the highest probability, and tiles were mosaicked to obtain wall-to-wall classifications. Spatial accuracy was then refined through post-processing, in which boundary errors, fragmented patches, and suspected omissions were manually corrected using sub-meter Google Earth imagery and existing mangrove datasets. For years without historical sub-meter imagery, alternative high-resolution data and ancillary information were used. All edits were cross-checked by two experienced field researchers, yielding the Sub-meter Time-series Mangrove Map (STMM) for China from 1990 to 2020.

2.4 Accuracy assessment

To evaluate SMTLM's effectiveness, we assessed the three transfer learning strategies' accuracy using mIoU, F1-score, and Precision, calculated on the fine-tuning dataset's validation subset. For objective classification performance of STMM products, quantitative evaluation employed the testing dataset (Section 2.2.3) with Overall Accuracy (OA), Producer's Accuracy (PA), User's Accuracy (UA), and F1-score; each metric is confined to the interval 0-1, and larger values correspond to better classification performance.

3. Results

3.1 Evaluation of transfer learning strategies

Fig. 5 compares the performance of DTL, PFT, and LFT in long-term mangrove mapping. LFT consistently outperformed the other two strategies across all evaluation metrics, achieving the highest mIoU, F1-score, and Precision. On average, LFT improved mIoU by about 2.6% over PFT and 4.9% over DTL, and yielded F1-score gains of 1.3% and 4.9%, respectively. Moreover, DTL and PFT showed substantial accuracy drops in early years such as 1990, while LFT maintained stable performance across all periods, demonstrating superior temporal robustness and transferability.

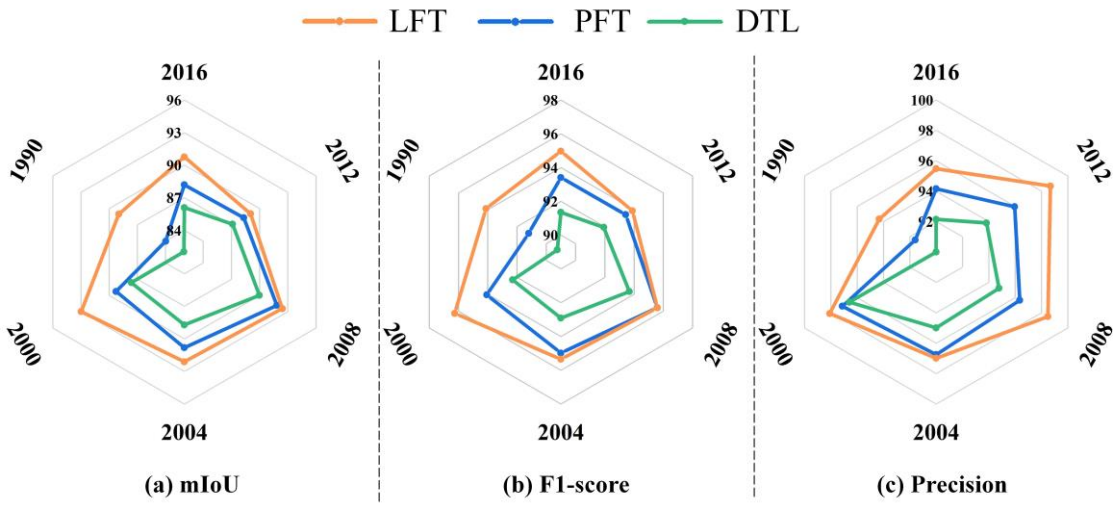

Fig. 5. Comparison of mIoU (%), F1-score (%), and Precision (%) among DTL, PFT,

and LFT.

3.2 Accuracy evaluation

Table 3 summarizes the accuracy of STMM products across years. The results demonstrate consistently high classification performance, with OA ranging from 93.4% (1990) to 97.2% (2020). PA for mangrove class exceeded 88% in all years, while UA was consistently above 97.9%, indicating robust detection with minimal omission and commission errors. The F1-score remained above 0.93 throughout, reaching its maximum of 0.97 in 2020. Non-mangrove classification also achieved stable performance, with PA and UA generally above 89%. These findings confirm that STMM maintains reliable performance and strong temporal stability in mangrove mapping.

Table 3

Classification performance metrics of the STMM.

Product	Class	PA (%)	UA (%)	OA (%)	F1-score
STMM_2020	Mangrove	95.6	98.8	97.2	0.97
	Non-mangrove	98.8	95.7		
STMM_2016	Mangrove	90.3	98.9	94.7	0.94
	Non-mangrove	99.0	91.1		
STMM_2012	Mangrove	92.7	99.1	96.0	0.96
	Non-mangrove	99.2	93.2		
STMM_2008	Mangrove	92.1	99.2	95.7	0.96
	Non-mangrove	99.2	92.6		
STMM_2004	Mangrove	88.4	99.4	93.9	0.94
	Non-mangrove	99.4	89.5		
STMM_2000	Mangrove	90.4	99.1	94.8	0.95
	Non-mangrove	99.2	91.2		
STMM_1990	Mangrove	88.7	97.9	93.4	0.93
	Non-mangrove	98.1	89.7		

3.3 Spatial structures and details

To assess differences in spatial details between STMM and existing mangrove products, we compared edge delineation, interior structures, and small patches. Fig. 6 highlights edge variations among STMM, HGMF, GMW, MC, and CAS, overlaid on a 0.6 m RGB basemap, for three edge types: tidal flats (Fig. 6(a)), water (Fig. 6(b)), and *Spartina alterniflora* (Fig. 6(c)). STMM achieved superior boundary accuracy, and the other products frequently misclassified large *Spartina alterniflora* areas as mangroves. Fig. 7 demonstrates internal feature detection, including open spaces and creeks; STMM delineated tidal channels 10 m wide and open areas 0.15 ha, whereas alternatives typically omitted these. Fig. 8 compares small patch identification: STMM excelled in detecting fragmented patches of mangroves or *Spartina alterniflora*, unlike other products, which often overlooked or misclassified them due to resolution constraints.

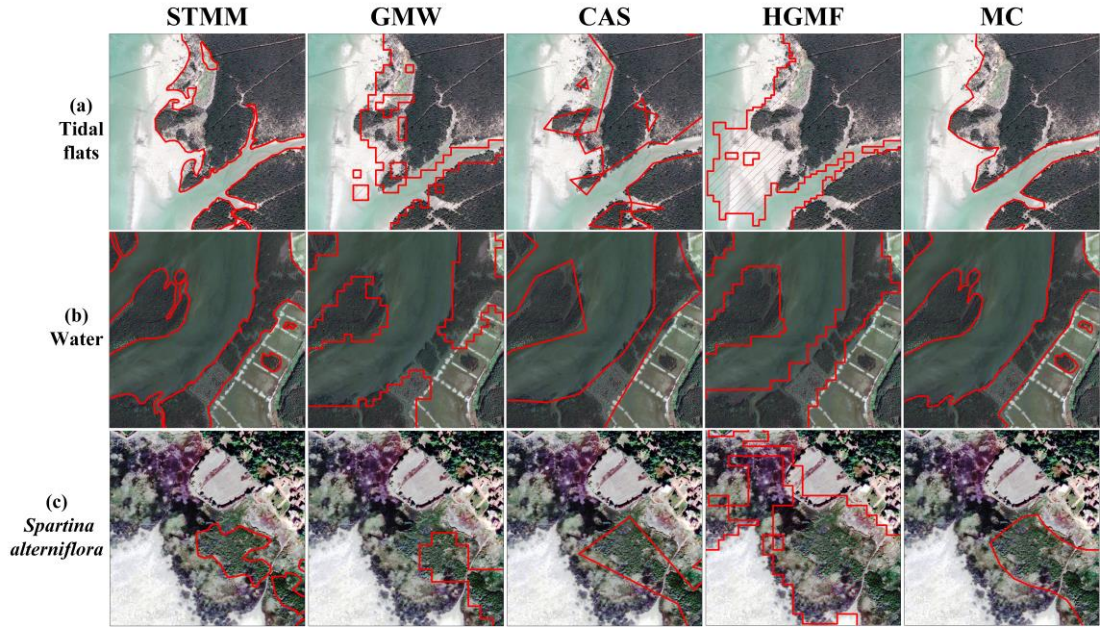

Fig. 6. Edge delineation of mangrove communities in STMM and other products.

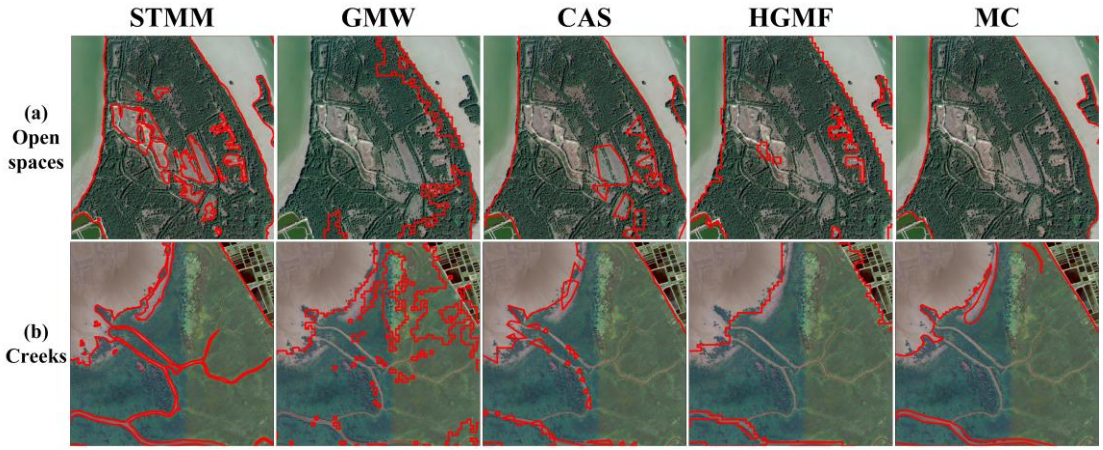

Fig. 7. Internal structure representation of mangrove communities in STMM and other products.

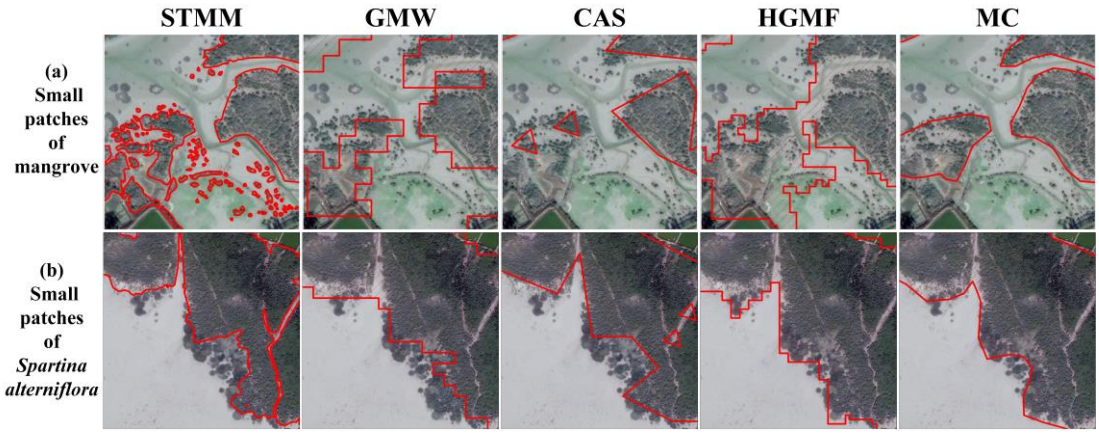

Fig. 8. Detection of small mangrove patches in STMM and other products.

3.4 Spatio-temporal evolution of mangrove forests in China

Fig. 9 depicts the temporal dynamics of mangrove distribution in China, revealing distinct change patterns across periods. From 1990 to 2020, the total mangrove area first declined and then increased. Mangrove extent decreased from 16,285 ha in 1990 to 14,316 ha in 2000, representing a 12% decline, and then recovered to 29,413 ha by 2020, corresponding to an overall increase of approximately 105.4%.

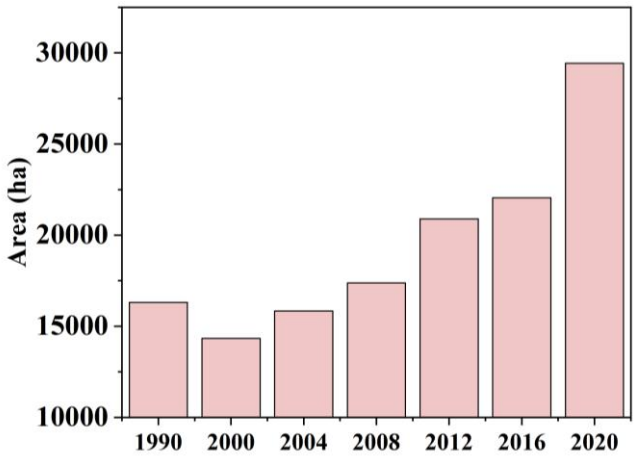

Fig. 9. Total mangrove area in China across seven periods.

Fig. 10 displays changes in mangrove extent among China's coastal regions between 1990 and 2020, highlighting clear spatiotemporal variability. Macao was merged into Guangdong statistics due to its small mangrove extent. Guangxi shows sustained expansion, with mangrove area increasing by about 213% over the study period. Guangdong recorded a 36% reduction in mangrove area between 1990 and 2000, and then a 145% expansion from 2000 to 2020. Hainan exhibits a 20% decrease from 1990 to 2004 and a subsequent 41% increase by 2020, indicating recent restoration gains. Fujian and Taiwan show overall growth, whereas Zhejiang and Hong Kong display relatively minor fluctuations.

Fig. 10. Temporal and provincial variation in mangrove in China (1990-2020).

3.5 Comparison with existing products

Table 4 presents a comparison of mangrove patch counts among different products. STMM detected substantially more mangrove patches than CAS and MC, with relative increases of 38%-306% and 114%-148%, respectively. When compared with GMW, STMM also showed higher patch counts of 14%-78% in overlapping years, demonstrating its superior performance in identifying fragmented and boundary-adjacent mangrove patches.

Table 4

Comparison of patches counts measured by STMM and other products.

Year	STMM	CAS	GMW	MC
1990	5181	1855	--	2086
2000	6708	2465	--	2769
2008	9906	2441	12030	--
2012	11432	--	--	5353
2016	11796	--	10320	--
2020	16414	11932	9228	--

Fig. 11 illustrates temporal area trends. STMM indicates a 105.4% increase in mangrove extent from 2000 to 2020, surpassing MC (26.8%) and CAS (23.3%) gains; its expansion rate is 3.9 times that of MC and 4.5 times that of CAS. In contrast, GMW shows stability from 1996 to 2020 without upward trends. Fig. 12 compares mangrove areas from STMM and other products for matching years, with percentages computed using STMM as the denominator (e.g., 117% = 19,089 ÷ 16,285 × 100%). Relative to STMM, CAS exhibits 54%-76% spatial overlap, with commissions of 3,847 ha (2020) to 11,627 ha (1990), omissions of 4,195 ha (2000) to 10,184 ha (2020), and differences of 9,496 ha (2016, 43%) to 19,089 ha (1990, 117%). MC shows 69%-78% overlap with 59%-99% differences, while GMW has the lowest overlap (47%-62%) and differences of 83%-107%. Commission denotes non-mangrove areas misclassified as mangroves; omission indicates mangroves misclassified as other land-cover types.

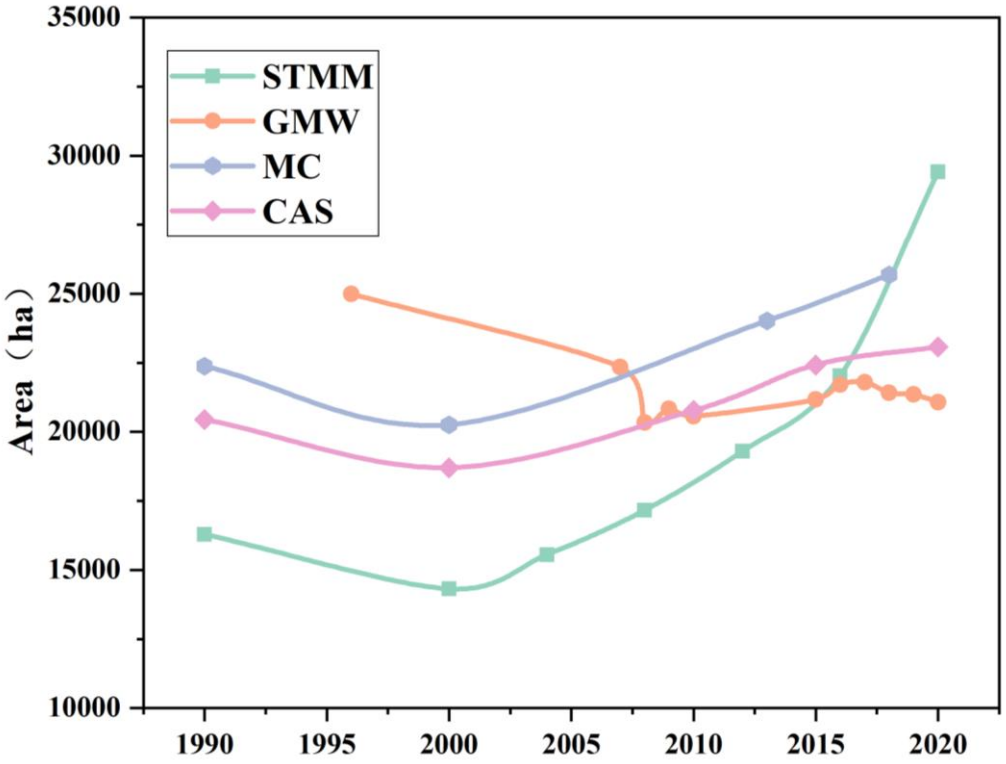

Fig. 11. Trend analysis of the existing products.

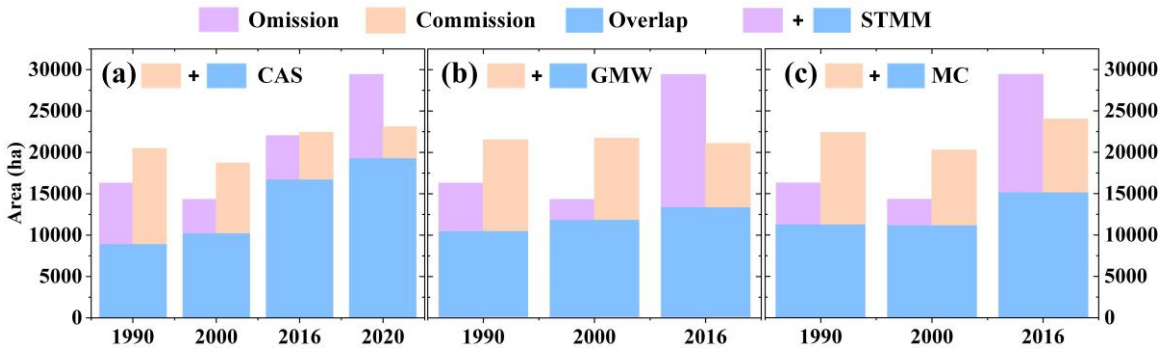

Fig. 12. Comparison of area statistics. (a) STMM and CAS, (b) STMM and GMW, (c) STMM and MC.

4. Discussion

4.1 Merits of SMTLM

Efficient use of limited historical samples is critical for long-term mangrove mapping. This challenge places two key requirements on mapping approaches: achieving high accuracy with scarce training samples (Dutta and Das, 2023) and mitigating domain shifts arising from inter-annual variations (Wang et al., 2023).

SMTLM systematically addresses these issues and offers a robust solution for large-scale mapping.

SMTLM mitigates the scarcity of historical samples through transfer learning. Traditional pixel-based and object-based classification methods can support long-term mangrove mapping (Xue and Qian, 2022; Xiao et al., 2021). However, they require large quantities of training samples (Khushbu et al., 2021). The lack of VHR historical imagery hinders the generation of sufficient samples, making these methods difficult to apply directly to long-term sub-meter mapping tasks. The semi-automatic sub-meter mapping method proposed by Tian et al. (2025) can generate representative training data, yet it depends on GE sub-meter imagery and existing mangrove products as references, which are often absent in earlier years, restricting its applicability to long-term mapping. To this end, SMTLM first pre-trains SegFormer on extensive PY samples to learn generalized mangrove representations, and subsequently fine-tuning the network with a small number of TY samples to adapt to the target domain while preserving previously learned features (Li et al., 2022b). This approach reduces sample requirements while sustaining high accuracy. As shown in Table 2 and Table **3**, reductions of 60%-80% in sample size still yield comparable to full-sample training. This strategy significantly decreases dependence on annotated samples and improves efficiency, which is particularly advantageous for historical years with limited available data (Lin et al., 2023).

SMTLM's LFT strategy alleviate domain shift from different year image. Transfer learning strategy selection markedly affects model performance. Therefore, we compared DTL, PFT, and LFT. Results indicated LFT superior across metrics (Fig. 5). DTL computationally efficient, but it degrades under spectral or structural domain discrepancies. For example, Xie et al. (2016) showed CNN feature transfer from natural to remote sensing images causes mismatch and accuracy decline, underscoring DTL limits. PFT updates high-level layers while freezing low-level ones, assuming transferable low-level features like texture or edges (Oquab et al., 2014). However, Yosinski et al. (2014) noted freezing shallow layers hinders adaptation amid differing low-level spectral patterns between years or sensors, prevalent in long-term mangrove

mapping. LFT progressively unfreezes layers top-down, enabling gradual semantic, structural, and spectral adaptation (Kornblith et al., 2019). This hierarchical approach avoids abrupt shifts, preserves PY knowledge stability, and adapts to TY variations. This alignment of model features with TY samples ensures long-term stability and robustness in multi-temporal remote sensing.

4.2 Merits of STMM

The Sub-meter Time-series Mangrove Map (STMM) provides comprehensive and reliable data, enabling precise fine-scale mangrove and ecosystem monitoring. The key advantages of STMM can be summarized as follows: classification accuracy and long-term temporal trend representation. We analyze the factors driving these advancements and their ecological implications.

STMM achieves exceptional accuracy (Table 3), attributed to three critical factors: sample, model, and transfer learning strategy. First, we constructed a large and representative sub-meter mangrove training set based on LSMM, enabling robust pre-training and cross-year model transfer. The quality and diversity of pre-training samples play a decisive role in transfer learning performance (Ma et al., 2024). The LSMM dataset, as a sub-meter product, supplies abundant, well-distributed samples and fine spatial detail, enabling the model to learn subtle structural and boundary characteristics within mangrove stands. Second, the use of SegFormer (Section 2.3.2), which integrates multi-scale feature extraction with attention mechanisms, is well suited to the complex patch patterns and boundary geometries typical of mangrove landscapes (Song et al., 2025). Third, systematic comparison of transfer learning schemes confirmed the advantage of LFT for long-term mapping. As shown in Fig. 5, LFT improves mIoU by about 2.6% relative to PFT and 4.9% relative to DTL, with corresponding F1 gains of 1.3% and 4.9%, respectively, further enhancing the accuracy of STMM.

STMM supports precise monitoring of mangrove dynamics and yields area estimates that closely approximate actual statistics. Taking CAS as an example, its lower classification accuracy and coarser spatial detail (Table 4; Fig. 8) introduce

substantial biases in mangrove area. Because commission and omission partly offset, CAS reports 4,386 ha more mangroves than STMM in 2000 but 6,337 ha fewer in 2020. Consequently, estimates of 21st-century change diverge markedly: CAS indicates a 23% increase, whereas STMM suggests a 105% expansion, about 4.5 times larger. Spatial discrepancies between CAS and STMM, defined as the sum of commission and omission errors, range from 9,496 ha in 2016 to 19,089 ha in 1990, corresponding to 43% to 117% of the STMM-derived mangrove area. Patch counts, an important indicator of mangrove fragmentation (Ximenes et al., 2023), also differ substantially: STMM maps 38% to 306% more patches than CAS (Table 4) , thereby increasing the reliability of subsequent ecological analyses. Collectively, these findings highlight limitations of current products and indicate that temporally continuous, sub-meter datasets are required for reliable area estimation and fine-scale spatial analysis of mangrove ecosystems.

4.3 Limitations

Although the proposed SMTLM effectively alleviates the issue of sample scarcity in historical mangrove mapping and enables the generation of STMM, several limitations still exist.

SMTLM faces two primary limitations. First, to minimize inter-sensor discrepancies impairing model transferability, we used only Landsat imagery, excluding others like Sentinel-2. Although resampling improves visual smoothness, the intrinsic 30 m resolution constrains the minimum detectable patch size. Future work could integrate historical high-resolution imagery or apply super-resolution reconstruction to enhance spatial detail (Chen et al., 2024; Li et al., 2022a) However, super-resolution was not employed in this study because Landsat's six spectral bands are not consistently available in higher-resolution datasets, which would compromise the consistency of input features (Yang et al., 2024). Second, since pre-training composite imagery includes pixels from adjacent years in some areas, temporal misalignment between samples and corresponding input images may cause minor spatial inconsistencies.

Propagation errors during training may weaken the model's cross-year generalization ability. In the future, emphasis should be placed on supplementing data from different sources concurrently to ensure temporal consistency (Zhou et al., 2025; Huo et al.,2024).

STMM also has two limitations. First, there may still be minor omissions or misclassifications. Although multiple existing mangrove products combined with manual interpretation were used to delineate the study area, it is possible that some mangrove habitats were excluded. In addition, in the post-processing stage, visual verification is difficult for areas with complex ecological environments, and errors may exist. Nevertheless, such instances are rare and have a negligible impact on overall statistics. Second, although STMM performs well in terms of spatial details, approaching the performance of the 2-m resolution product MC, it may not be sufficient to achieve genuine sub-meter accuracy due to the inherent resolution limitation of Landsat imagery. Further work could integrate multi-source time-series high-resolution remote sensing data (Fu et al., 2024; Sun et al., 2025), employ advanced super-resolution reconstruction technology, and supplement sub-meter feature details to achieve mapping accuracy closer to the sub-meter level.

5. Conclusion

This study developed the Sub-meter Mangrove Transfer Learning Mapping (SMTLM) framework, leveraging the SegFormer deep learning model. Pre-trained on extensive 2020 sub-meter mangrove samples, the model was fine-tuned using limited transfer-year samples via the LFT strategy. SMTLM mitigates the scarcity of high-quality historical samples and generates the Sub-meter Time-series Mangrove Map (STMM). STMM outperforms existing products (GMW, CAS, and HGMF) in spatial accuracy and detail, detecting 151%-198% more mangrove patches. It shows that mangrove extent increased by 105.4% from 2000 to 2020, which is 3.9 times higher than the growth reported by MC and 4.5 times higher than that reported by CAS for the same period. In conclusion, this work demonstrates the efficacy of SegFormer and LFT in remote sensing-based mangrove mapping, providing a novel solution to historical

sample shortages. STMM offers a vital benchmark for mangrove conservation and restoration research in China.

Data availability

The complete STMM dataset is available at https://doi.org/10.5281/zenodo.17867080.

Acknowledgments

This work was supported by the National Natural Science Foundation of China (Grant Nos. 42171330 and 42571440) and the Beijing Natural Science Foundation (Grant No. L251047).

References

Bunting, P., Rosenqvist, A., Hilarides, L., Lucas, R.M., Thomas, N., Tadono, T., Worthington, T.A., Spalding, M., Murray, N.J., Rebelo, L.-M., 2022. Global mangrove extent change 1996-2020: Global Mangrove Watch version 3.0. Remote Sens. 14(15), 3657.

Bunting, P., Rosenqvist, A., Lucas, R.M., Rebelo, L.-M., Hilarides, L., Thomas, N., Hardy, A., Itoh, T., Shimada, M., and Finlayson, C.M., 2018. The Global Mangrove Watch - a new 2010 global baseline of mangrove extent. Remote Sens. 10(10), 1669.

Chen, B., Xiao, X., Li, X., Pan, L., Doughty, R., Ma, J., Dong, J., Qin, Y., Zhao, B., Wu, Z., 2017. A mangrove forest map of China in 2015: Analysis of time series Landsat 7/8 and Sentinel-1A imagery in Google Earth Engine cloud computing platform. ISPRS J. Photogramm. Remote Sens. 131, 104-120.

Chen, W., Shi, C., 2023. Fine-scale mapping of *Spartina alterniflora*-invaded mangrove forests with multi-temporal WorldView–Sentinel-2 data fusion. Remote Sens. Environ. 295, 113690.

Chen, W., Tian, J., Song, J., Li, X., Ke, Y., Zhu, L., Yu, Y., Ou, Y., Gong, H., 2024. A novel super-resolution model for 10-m mangrove mapping with Landsat-5. IEEE Trans. Geosci. Remote Sens. 62, 1-12.

Dutta, S., Das, M., 2023. Remote sensing scene classification under scarcity of labelled samples—A survey of the state-of-the-arts. Comput. Geosci. 171, 105295.

Fu, B., Zhang, S., Li, H., Yao, H., Sun, W., Jia, M., Yang, Y., He, H., Li, Y., 2024. Exploring the effects of different combination ratios of multi-source remote sensing images on mangrove communities classification. Int. J. Appl. Earth Obs. Geoinf. 134, 104197.

Giri, C., Long, J., Abbas, S., Murali, R.M., Qamer, F.M., Pengra, B., Thau, D., 2015. Distribution and dynamics of mangrove forests of South Asia. J. Environ. Manage. 148, 101-111.

Hamilton, S.E., Casey, D., 2016. Creation of a high spatio-temporal resolution global database of continuous mangrove forest cover for the 21st century (CGMFC-21). Global Ecol. Biogeogr. 25, 729-738.

Hu, L., Li, W., Xu, B., 2018. Monitoring mangrove forest change in China from 1990 to 2015 using Landsat-derived spectral-temporal variability metrics. Int. J. Appl. Earth Obs. Geoinf. 73, 88-98.

Huo, X., Niu, Z., Liu, L., Jing, Y., 2024. Integration of ecological knowledge with Google Earth Engine for diverse wetland sampling in global mapping. Int. J. Appl. Earth Obs. Geoinf. 134, 104249.

Jia, M., Wang, Z., Mao, D., Ren, C., Song, K., Zhao, C., Wang, C., Xiao, X., Wang, Y., 2023. Mapping global distribution of mangrove forests at 10-m resolution. Sci. Bull. 68, 1306-1316.

Jia, M., Wang, Z., Zhang, Y., Mao, D., Wang, C., 2018. Monitoring loss and recovery of mangrove forests during 42 years: The achievements of mangrove conservation in China. Int. J. Appl. Earth Obs. Geoinf. 73, 535-545.

Khushbu, M., Seema, M., Nilima, C., 2021. Remote sensing techniques: mapping and monitoring of mangrove ecosystem—a review. Complex Intell. Syst. 7, 2797-2818.

Kornblith, S., Shlens, J., Le, Q.V., 2019. Do better ImageNet models transfer better? In: Proceedings of the IEEE/CVF Conference on Computer Vision and Pattern Recognition, Long Beach, CA, USA, 16-20 June, pp. 2661-2671.

Lei, L., Wang, X., Zhang, L., Hu, X., Zhong, Y., 2024. CROPUP: Historical products are all you need? An end-to-end cross-year crop map updating framework without the need for

in situ samples. Remote Sens. Environ. 315, 114430.

Li, X., Tian, J., Li, X., Wang, L., Gong, H., Shi, C., Nie, S., Zhu, L., Chen, B., Pan, Y., 2022a. Developing a sub-meter phenological spectral feature for mapping poplars and willows in urban environment. ISPRS J. Photogramm. Remote Sens. 193, 77-89.

Li, Y., Fu, B., Sun, X., Fan, D., Wang, Y., He, H., Gao, E., He, W., Yao, Y., 2022b. Comparison of different transfer learning methods for classification of mangrove communities using MCCUNet and UAV multispectral images. Remote Sens. 14, 5533.

Lin, X., Cheng, Y., Chen, G., Chen, W., Chen, R., Gao, D., Zhang, Y., Wu, Y., 2023. Semantic segmentation of China's coastal wetlands based on Sentinel-2 and Segformer. Remote Sens. 15, 3714.

Ma, Y., Chen, S., Ermon, S., Lobell, D.B., 2024. Transfer learning in environmental remote sensing. Remote Sens. Environ. 301, 113924.

Matos, C.R.L., Berrêdo, J.F., Machado, W., Sanders, C.J., Metzger, E., Cohen, M.C.L., 2020. Carbon and nutrient accumulation in tropical mangrove creeks, Amazon region. Mar. Geol. 429, 106317.

Naushad, R., Kaur, T., Ghaderpour, E., 2021. Deep transfer learning for land use and land cover classification: A comparative study. Sensors 21, 8083.

Oquab, M., Bottou, L., Laptev, I., Sivic, J., 2014. Learning mid-level image representations using CNNs. In: Proceedings of the IEEE Conference on Computer Vision and Pattern Recognition, Columbus, OH, USA, 23-28 June, pp. 1717-1724.

Sun, Z., Jiang, W., Ling, Z., Sun, J., Zhang, Z., Huang, S., Li, Q., 2025. Rapid expansion of coastal mangrove forest in Guangxi Beibu Gulf: Patterns, drivers, and impacts. IEEE J. Sel. Top. Appl. Earth Obs. Remote Sens. 18, 510-522.

Song, J., Tian, J., Zhu, L., Zhou, B., Qu, X., Wang, C., Luo, N., Zhang, Z., Guo, L., Gao, M., Li, X., Gong, H., 2025. Sub-metre surface water mapping using Sentinel-1/2 with integrated super-resolution and deep learning. Int. J. Remote Sens., 1-23.

Tan, J., Li, J., Ma, T., Yan, X., Huo, Z., 2025. Leveraging Sentinel-1/2 time series and deep learning for accurate forest tree species mapping. Front. For. Global Change 8, 1599510.

Tian, J., Wang, L., Diao, C., Zhang, Y., Jia, M., Zhu, L., Xu, M., Li, X., Gong, H., 2025. National scale sub-meter mangrove mapping using an augmented border training sample method.

ISPRS J. Photogramm. Remote Sens. 220, 156-171.

Tian, J., Wang, L., Li, X., Gong, H., Shi, C., Zhong, R., Liu, X., 2017. Comparison of UAV and WorldView-2 imagery for mapping leaf area index of mangrove forest. Int. J. Appl. Earth Obs. Geoinf. 61, 22-31.

Tian, J., Wang, L., Yin, D., Li, X., Diao, C., Gong, H., Shi, C., Menenti, M., Ge, Y., Nie, S., 2020. Development of spectral-phenological features for deep learning to understand *Spartina alterniflora* invasion. Remote Sens. Environ. 242, 111745.

Tran, T.V., Reef, R., Zhu, X., 2022. A review of spectral indices for mangrove remote sensing. Remote Sens. 14, 4868.

Wang, L., Jia, M., Yin, D., Tian, J., 2019. A review of remote sensing for mangrove forests: 1956-2018. Remote Sens. Environ. 231, 111223.

Wang, Y., Feng, L., Zhang, Z., Tian, F., 2023. An unsupervised domain adaptation deep learning method for spatial and temporal transferable crop type mapping using Sentinel-2 imagery. ISPRS J. Photogramm. Remote Sens. 199, 102-117.

Xiao, H., Su, F., Fu, D., Lyne, V., Liu, G., Pan, T., Teng, J., 2021. Optimal and robust vegetation mapping in complex environments using multiple satellite imagery: Application to mangroves in Southeast Asia. Int. J. Appl. Earth Obs. Geoinf. 99, 102320.

Xie, E., Wang, W., Yu, Z., Anandkumar, A., Alvarez, J.M., Luo, P., 2021. SegFormer: Simple and efficient design for semantic segmentation with transformers. Adv. Neural Inf. Process. Syst. 34, 12077-12090.

Xie, M., Jean, N., Burke, M., Lobell, D., Ermon, S., 2016. Transfer learning from deep features for remote sensing and poverty mapping. In: Proceedings of the Thirtieth AAAI Conference on Artificial Intelligence (AAAI 2016), AAAI Press, Phoenix, AZ, USA, 12-17 February, pp. 3929-3935.

Ximenes, A.C., Cavanaugh, K.C., Arvor, D., Murdiyarso, D., Thomas, N., Arcoverde, G.F.B., da Conceição Bispo, P., Van der Stocken, T., 2023. A comparison of global mangrove maps: Assessing spatial and bioclimatic discrepancies at poleward range limits. Sci. Total Environ. 860, 160380.

Xu, X., Fu, D., Su, F., Lyne, V., Yu, H., Tang, J., Hong, X., Wang, J., 2024. Global distribution and decline of mangrove coastal protection extends far beyond area loss. Nat. Commun.

15, 10267.

Xue, Z. and Qian, S., 2022. Generalized composite mangrove index for mapping mangroves using Sentinel-2 time series data. IEEE J. Sel. Top. Appl. Earth Obs. Remote Sens. 15, 5131-5146.

Yang, G., Huang, K., Sun, W., Meng, X., Mao, D., Ge, Y., 2022. Enhanced mangrove vegetation index based on hyperspectral images for mapping mangrove. ISPRS J. Photogramm. Remote Sens. 189, 236-254.

Yang, X., Zhu, Z., Kroeger, K.D., Qiu, S., Covington, S., Conrad, J.R., Zhu, Z., 2024. Tracking mangrove condition changes using dense Landsat time series. Remote Sens. Environ. 315, 114461.

Ye, L., Weng, Q., 2025. A hybrid neural network for mangrove mapping considering tide states using Sentinel-2 imagery. Remote Sens. Environ. 329, 114917.

Yosinski, J., Clune, J., Bengio, Y., Lipson, H., 2014. How transferable are features in deep neural networks. In: Advances in Neural Information Processing Systems 27, Montreal, Canada, pp. 3320–3328.

Zhang, T., Hu, S., He, Y., You, S., Yang, X., Gan, Y., Liu, A., 2021. A fine-scale mangrove map of China derived from 2-meter resolution satellite observations and field data. ISPRS Int. J. Geo-Inf. 10, 92.

Zhao, C., Qin, C.-Z., 2020. 10-m-resolution mangrove maps of China derived from multi-source and multi-temporal satellite observations. ISPRS J. Photogramm. Remote Sens. 169, 389-405.

Zhou, B., Xu, M., Tian, J., Huang, Y., Song, J., Zhu, L., Zhu, X., Qu, X., Zhang, L., Li, X., 2024. Mapping the invasive Spartina alterniflora in sub-meter level with improved phenological spectral features and deep learning method. Int. J. Digit. Earth 17, 2434634.

Zhou, B., Xu, M., Tian, J., Jia, M., Mao, D., Cheng, K., Zhu, X., Jiang, H., Song, J., Ke, Y., Zhang, Z., Huang, Y., Wei, M., Zhu, L., Li, X., Gong, H., 2025. National-scale sub-meter mapping of *Spartina alterniflora* in mainland China 2020. Earth Syst. Sci. Data Discuss. [preprint]. https://doi.org/10.5194/essd-2025-436.

Zhuang, F., Qi, Z., Duan, K., Xi, D., Zhu, Y., Zhu, H., Xiong, H., He, Q., 2020. A comprehensive survey on transfer learning. Proc. IEEE 109, 43-76.